AIAA JOURNAL
Vol. 40, No. 3, March 2002

Noise from Fine-Scale Turbulence of Nonaxisymmetric Jets

Christopher K. W. Tam* and Nikolai N. Pastouchenko†
Florida State University, Tallahassee, Florida 32306-4510

The noise from the fine-scale turbulence of high-speed nonaxisymmetric jets is considered. A prediction method is developed by extending the work of Tam and Auriault (Tam, C. K. W., and Auriault, L., "Jet Mixing Noise from Fine-Scale Turbulence," *AIAA Journal*, Vol. 37, No. 2, 1999, pp. 145–153). A set of improved numerical boundary conditions for use in nonaxisymmetric jet mean flow and turbulence calculation is developed. These new boundary conditions allow the computation to be carried out in a smaller computation domain. It is known that nonaxisymmetric mean flow has a significant impact on the radiated noise spectrum and directivity through refraction. In the Tam and Auriault theory, this effect is accounted for by means of the adjoint Green's function. Here the adjoint Green's function method is extended to nonaxisymmetric mean flows. The adjoint Green's function is first recast into the solution of a sound scattering problem. The sound scattering problem is then solved computationally by computational aeroacoustics methods. Extensive comparisons between calculated and experimentally measured jet noise spectra are presented. They include both rectangular and elliptic jets at supersonic and subsonic Mach numbers. Good agreements are found even for jets with very large aspect ratio.

Nomenclature

c_v	=	specific heat at constant volume
D_j	=	jet diameter (fully expanded if jet is supersonic)
f, ω	=	frequency and angular frequency
k	=	turbulence kinetic energy
Pr	=	Prandtl number
p	=	pressure
(R, Θ, ϕ)	=	spherical polar coordinates
(r, ϕ, x)	=	cylindrical coordinates
T	=	temperature
u_j	=	jet velocity (fully expanded if jet is supersonic)
(u, v, w)	=	velocity components
(u_a, v_a, w_a, p_a)	=	adjoint variables
$(u_\infty, \rho_\infty, p_\infty, T_\infty)$	=	ambient conditions
(x, y, z, t)	=	Cartesian coordinates and time
(α, β, Ω)	=	wave number in x and y directions and angular frequency
γ	=	ratio of specific heat
ε	=	dissipation rate of the k–ε turbulence model
κ	=	wave number of waves in perfectly matched layer
ν	=	molecular viscosity
ν_t	=	turbulent viscosity
ρ	=	density
σ	=	damping constant

I. Introduction

A SEARCH through the literature reveals that there is no reliable nonaxisymmetric jet noise prediction theory at the present time. The objective of this investigation is to extend the recently developed semi-empirical jet noise theory of Tam and Auriault[1] to nonaxisymmetric jets. In the original work, only axisymmetric jets were considered.

The Tam and Auriault theory[1] calculates only the noise from the fine-scale turbulence of a jet. The theory first separates out the fine-scale turbulence from the flow and acoustics by spatial filtering. The spatially filtered governing equations have essentially the same form as the Reynolds-averaged Navier–Stokes equations (RANS). Tam and Auriault suggested[1] that the dominant part of fine-scale turbulence mixing noise is generated by the unsteady turbulence kinetic energy. Refraction of sound by the flow and density gradients of the jet is included in the theory through the use of the adjoint Green's function. Information concerning the fine-scale turbulence is supplied by the semi-empirical k–ε turbulence model. Aside from the inherent empirical constants of the k–ε model, the theory contains three empirical constants of its own. Two of these constants are used to establish the length scales and timescales of the fine-scale turbulence. The turbulence kinetic energy computed by the k–ε model includes both the large- and fine-scale turbulence of the jet. The third constant effectively assigns the proper fraction of the turbulence kinetic energy k to the fine-scale turbulence. The three constants were found by best fit to the jet noise data of the Jet Noise Laboratory of NASA Langley Research Center.[2,3] Tam and Auriault[1] applied their theory to the prediction of cold jet noise spectra over a wide range of Mach numbers from 0.3 to 2.0. Note that the sound pressure level (SPL) of a Mach 2.0 jet is about 60 dB higher than that of a Mach 0.3 jet. Thus, the experimental data cover a very large range of SPLs. The predicted spectra agreed well with experimental measurements. Tam and Auriault also compared the calculated noise spectra with hot supersonic jet noise data at Mach 1.5 and 2.0. Good agreements were again found. The temperature ratio of the data varied from 1.0 to 4.9. This temperature range brackets the operating conditions of all modern day commercial jet engines.

Most recently, Tam et al.[4] used the theory to calculate the noise from jets in simulated forward flight. Experimentally, it is known that for each 0.2 increase in forward flight Mach number, there is a reduction of sideline noise of 4–4.5 dB. This is a large change in jet noise level. Tam et al. compared the calculated noise spectra for a Mach 1.5 jet at simulated forward flight Mach number 0.0, 0.2, and 0.4 with the measurements of Norum and Brown.[5] Excellent agreements were found. They[4] also compared the calculated noise spectra for subsonic jets in forward flight with the data of Ref. 6. Again good agreements were found.

To calculate the noise from nonaxisymmetric jets, two crucial requirements must be met. First, one must compute the mean flow and the turbulence quantities needed for the noise source model. Second, a method to calculate the flow refraction effects over the entire frequency spectrum of jet noise has to be developed.

The Tam and Auriault theory[1] relies on the k–ε turbulence model for input on jet mean flow, noise source intensity and the characteristic length scales and timescales of the turbulence. The constants of the k–ε model are, however, not those of the standard model. Tam and Auriault chose to adopt the values suggested by Thies and

Received 22 March 2001; revision received 4 September 2001; accepted for publication 4 September 2001.

*Robert O. Lawton Distinguished Professor, Department of Mathematics. Fellow AIAA.
†Graduate Student, Department of Mathematics.

Tam.[7] Thies and Tam observed that the large turbulence structures of a flow, having dimensions comparable to the mean flow, would likely be affected by the flow geometry and boundary conditions. Their dynamics and characteristics are, therefore, flow specific. In other words, the large-scale turbulence is not universal. The constants of the standard model were calibrated by data from low-speed boundary-layer and two-dimensional mixing layers. Thus, they are not necessarily suitable for high-speed jets. Indeed, past attempts to use the standard model to predict jet mean flow profiles did not give satisfactory results. Thies and Tam then suggested that if one restricted one's consideration to a specific class of flows with similar characteristics, such as jet flow alone, it would be reasonable to expect a single set of constants to work for all of the flows within the class. They recalibrated the constants for jet flows using a large database. Here we will use the values of the constants they recommend.

To calculate the mean flow, Thies and Tam[7] solved the parabolized RANS equations supplemented by the k–ε model. They employed the highly accurate dispersion-relation-preserving (DRP) scheme[8] for numerical solution. In this work, the mean flows of nonaxisymmetric jets are calculated essentially by the same procedure except that an improved set of boundary conditions is imposed. The new boundary conditions are developed to allow the computation to be carried out in a smaller computation domain. The formulation of the new boundary conditions is described in Sec. II.

The nonaxisymmetric mean flow of a jet, undoubtedly, has a significant impact on the noise directivity through refraction alone. Because low-frequency sound having long acoustic wavelength is less affected by refraction than high-frequency sound, the nonaxisymmetric mean flow will modify the noise spectrum in the far field. In the past, there have been many investigations on how best to quantify mean flow effects. Most of the approaches used asymptotic analysis based either on the low-frequency limit, for example, Goldstein,[9,10] or the high-frequency limit, for example, Balsa[11] and Goldstein.[12] Durbin[13,14] and Khavaran and Krejsa[15,16] considered the zero wavelength limit of geometric acoustics and ray tracing. However, jet noise is broadband, extending over a frequency range of almost three decades. It is difficult to justify the use of asymptotic results over such a broad frequency range. Typically, the Strouhal number, fD_j/u_j, at the peak of the noise spectrum is approximately equal to 0.3. For commercial jet engines, u_j is roughly equal to the speed of sound. Thus, the acoustic wavelength is as long as three jet diameters. This is definitely not in the high-frequency limit. Moreover, Khavaran[17] stated that the use of ray tracing was too computationally intensive to be practical.

In this paper, the flow effect is included in the theory through an extension of the adjoint Green's function approach of Tam and Auriault.[18] In Sec. III, it will be shown how the adjoint Green's function problem can be recast into a two-dimensional sound scattering problem. The sound scattering problem is then solved computationally in the time domain by the DRP scheme.[8] A perfectly matched layer (PML) boundary condition is enforced around the finite computation domain. The PML absorbs the scattered sound waves, thus preventing their reflection back into the computation domain. In this way, possible contamination of the numerical solution is avoided.

In Sec. IV, comparisons between computed noise spectra and experimental measurements are presented. Both rectangular and elliptic jets at supersonic and subsonic Mach numbers are included in the comparisons. Good agreements are found in all of the cases. The nonaxisymmetric features of the far-field noise spectra from large aspect ratio rectangular jets are correctly reproduced by the theory.

II. Mean Flow and Turbulence Computation

In this investigation, the mean flow and turbulence kinetic energy of nonaxisymmetric jets are calculated by the procedure used by Thies and Tam.[7] Thies and Tam employed the k–ε turbulence model but with a set of modified constants. They solved the parabolized RANS equations by means of the DRP scheme.[8] The solution starts at the nozzle exit plane and marches downstream. It is well known that the parabolized RANS equations are numerically unstable in regions without a mean flow. To stabilize the numerical solution, a small forward flight velocity, 2% or less of the jet exit velocity, is added outside the static jet. The computation is carried out in a finite domain in the y–z plane at each x station, where x is taken to be the flow direction. Because a finite domain is used, a set of boundary conditions must be imposed at the external boundaries. In the present investigation, a new set of boundary conditions are used. This set of boundary conditions is derived without invoking the far-field assumption $r \to \infty$. This allows the computation to be done in a smaller computation domain. The numerical results are found to be in good agreement with those obtained by the original code of Thies and Tam.[7] However, the computation time is reduced. In this section, the formulation of the new boundary conditions is presented.

The parabolized RANS equations including the Pope and Sarkar corrections (see Ref. 7) with respect to a Cartesian coordinate centered at the nozzle exit with the x axis pointing in the flow direction are

$$\frac{\partial u}{\partial x} = -\frac{v}{u}\frac{\partial u}{\partial y} - \frac{w}{u}\frac{\partial u}{\partial z} - \frac{1}{\rho u}\left[\frac{\partial}{\partial y}(\rho\tau_{xy}) + \frac{\partial}{\partial z}(\rho\tau_{xz})\right]$$

$$\frac{\partial v}{\partial x} = -\frac{v}{u}\frac{\partial v}{\partial y} - \frac{w}{u}\frac{\partial v}{\partial z} - \frac{1}{\rho u}\left[\frac{\partial p}{\partial y} + \frac{\partial}{\partial y}(\rho\tau_{yy}) + \frac{\partial}{\partial z}(\rho\tau_{yz})\right]$$

$$\frac{\partial w}{\partial x} = -\frac{v}{u}\frac{\partial w}{\partial y} - \frac{w}{u}\frac{\partial w}{\partial z} - \frac{1}{\rho u}\left[\frac{\partial p}{\partial z} + \frac{\partial}{\partial y}(\rho\tau_{yz}) + \frac{\partial}{\partial z}(\rho\tau_{zz})\right]$$

$$\frac{\partial T}{\partial x} = -\frac{v}{u}\frac{\partial T}{\partial y} - \frac{w}{u}\frac{\partial T}{\partial z} - \frac{(\gamma-1)}{u}T\left(\frac{\partial u}{\partial x} + \frac{\partial v}{\partial y} + \frac{\partial w}{\partial z}\right) + \frac{1}{c_v}\frac{\varepsilon}{u} + \frac{\gamma}{Pr}\frac{1}{\rho u}\left[\frac{\partial}{\partial y}\left(\rho\nu_t\frac{\partial T}{\partial y}\right) + \frac{\partial}{\partial z}\left(\rho\nu_t\frac{\partial T}{\partial z}\right)\right]$$

$$\frac{\partial p}{\partial x} = -\frac{p}{u}\frac{\partial u}{\partial x} + \frac{p}{T}\frac{\partial T}{\partial x} - \frac{v}{u}\frac{\partial p}{\partial y} - \frac{p}{u}\frac{\partial v}{\partial y} + \frac{v}{u}\frac{p}{T}\frac{\partial T}{\partial y} - \frac{w}{u}\frac{\partial p}{\partial z} - \frac{p}{u}\frac{\partial w}{\partial z} + \frac{w}{u}\frac{p}{T}\frac{\partial T}{\partial z}$$

$$\frac{\partial k}{\partial x} = -\frac{v}{u}\frac{\partial k}{\partial y} - \frac{w}{u}\frac{\partial k}{\partial z} - \frac{1}{u}\left[\tau_{xy}\frac{\partial u}{\partial y} + \tau_{xz}\frac{\partial u}{\partial z} + \tau_{yy}\frac{\partial v}{\partial y} + \tau_{yz}\frac{\partial v}{\partial z} + \tau_{zy}\frac{\partial w}{\partial y} + \tau_{zz}\frac{\partial w}{\partial z}\right] - \frac{\varepsilon}{u} + \frac{1}{\rho u\sigma_k}\left[\frac{\partial}{\partial y}\left(\rho\nu_t\frac{\partial k}{\partial y}\right) + \frac{\partial}{\partial z}\left(\rho\nu_t\frac{\partial k}{\partial z}\right)\right]$$

$$\frac{\partial \varepsilon_s}{\partial x} = -\frac{v}{u}\frac{\partial \varepsilon_s}{\partial y} - \frac{w}{u}\frac{\partial \varepsilon_s}{\partial z} - c_{\varepsilon 1}\frac{\varepsilon_s}{(k+k_0)}\frac{1}{u}\left[\tau^s_{xy}\frac{\partial u}{\partial y} + \tau^s_{xz}\frac{\partial u}{\partial z} + \tau^s_{yy}\frac{\partial v}{\partial y} + \tau^s_{yz}\frac{\partial v}{\partial z} + \tau^s_{zy}\frac{\partial w}{\partial y} + \tau^s_{zz}\frac{\partial w}{\partial z}\right] - (c_{\varepsilon 2} - c_{\varepsilon 3}\chi) \times \frac{\varepsilon_s^2}{(k+k_0)u} + \frac{1}{\rho u\sigma_\varepsilon}\left[\frac{\partial}{\partial y}\left(\rho\nu^s_t\frac{\partial \varepsilon_s}{\partial y}\right) + \frac{\partial}{\partial z}\left(\rho\nu^s_t\frac{\partial \varepsilon_s}{\partial z}\right)\right]$$

$$\rho = \frac{p}{(RT)}, \qquad \varepsilon = \varepsilon_s\left(1 + \alpha_1 M_t^2\right), \qquad M_t^2 = \frac{2k}{\gamma RT}$$

$$\nu_t = \frac{c_\mu k^2}{\varepsilon + \varepsilon_0}, \qquad \nu^s_t = \frac{c_\mu k^2}{\varepsilon_s + \varepsilon_0}$$

$$\tau_{ij} = -\nu_t\left(\frac{\partial u_i}{\partial x_j} + \frac{\partial u_j}{\partial x_i} - \frac{2}{3}\frac{\partial u_k}{\partial x_k}\delta_{ij}\right) + \frac{2}{3}k\delta_{ij}$$

$$\tau^s_{ij} = -\nu^s_t\left(\frac{\partial u_i}{\partial x_j} + \frac{\partial u_j}{\partial x_i} - \frac{2}{3}\frac{\partial u_k}{\partial x_k}\delta_{ij}\right) + \frac{2}{3}k\delta_{ij} \tag{1}$$

where all $\partial/\partial x \to 0$ in τ_{ij} and τ^s_{ij},

$$\chi = -\frac{1}{4}\left(\frac{k}{\varepsilon_s}\right)^3\left[\frac{\partial v}{\partial y}\left(\frac{\partial u}{\partial y}\right)^2+\frac{\partial w}{\partial z}\left(\frac{\partial u}{\partial z}\right)^2+\left(\frac{\partial v}{\partial z}+\frac{\partial w}{\partial y}\right)\frac{\partial u}{\partial y}\frac{\partial u}{\partial z}\right]$$

The constants are

$$c_\mu = 0.0874, \qquad \sigma_k = 0.324, \qquad \sigma_\varepsilon = 0.377, \qquad Pr = 0.422$$

$$c_{\varepsilon 1} = 1.4, \qquad c_{\varepsilon 2} = 2.02, \qquad c_{\varepsilon 3} = 0.822$$

$$k_0 = 10^{-6}, \qquad \varepsilon_0 = 10^{-4}, \qquad \alpha_1 = 0.518$$

(The two small positive numbers k_0 and ε_0 are inserted in the k–ε model to prevent division by zero.)

Outside the jet, the flow velocity and pressure and temperature perturbations are small. It is, therefore, sufficient to use the linearized form of Eq. (1). Also, note that in this region there is no turbulence or $k = \varepsilon = 0$. Let

$$u = u_\infty + u', \qquad v = v', \qquad w = w'$$

$$p = p_\infty + p', \qquad T = T_\infty + T' \tag{2}$$

Substitution of Eq. (2) into Eq. (1) and retaining only the lowest-order terms, the linearized equations are

$$u_\infty \frac{\partial u'}{\partial x} = 0 \tag{3}$$

$$u_\infty \frac{\partial v'}{\partial x} = -\frac{1}{\rho_\infty}\frac{\partial p'}{\partial y} \tag{4}$$

$$u_\infty \frac{\partial w'}{\partial x} = -\frac{1}{\rho_\infty}\frac{\partial p'}{\partial z} \tag{5}$$

$$u_\infty \frac{\partial T'}{\partial x} + (\gamma - 1)T_\infty\left(\frac{\partial u'}{\partial x}+\frac{\partial v'}{\partial y}+\frac{\partial w'}{\partial z}\right) = 0 \tag{6}$$

$$u_\infty \frac{\partial p'}{\partial x} - \frac{u_\infty p_\infty}{T_\infty}\frac{\partial T'}{\partial x} + p_\infty\left(\frac{\partial u'}{\partial x}+\frac{\partial v'}{\partial y}+\frac{\partial w'}{\partial z}\right) = 0 \tag{7}$$

The integral of Eq. (3) is

$$u' = 0 \tag{8}$$

Equations (6) and (7) may be integrated, by making use of Eq. (8), to yield the integral

$$T' = [(\gamma - 1)/\gamma](T_\infty/p_\infty)p' \tag{9}$$

Because of Eq. (9), the remaining unknown variables v', w', and p' are governed by Eqs. (4) and (5) and the following equation:

$$u_\infty \frac{\partial p'}{\partial x} + \gamma p_\infty\left(\frac{\partial v'}{\partial y}+\frac{\partial w'}{\partial z}\right) = 0 \tag{10}$$

At some distance away from the jet, the velocity and pressure fields are expected to be small and approximately axisymmetric. In this region, Eqs. (4), (5), and (10), when written in cylindrical coordinates (r, ϕ, x), have the form

$$u_\infty \frac{\partial v'_r}{\partial x} + \frac{1}{\rho_\infty}\frac{\partial p'}{\partial r} = 0 \tag{11}$$

$$u_\infty \frac{\partial p'}{\partial x} + \gamma p_\infty\left(\frac{\partial v'_r}{\partial r}+\frac{v'_r}{r}\right) = 0 \tag{12}$$

where v'_r is the radial velocity. If r is large, the last term of Eq. (12) may be neglected. In this case, Eqs. (11) and (12) become the simple wave equation, and the solution is a function of $\xi = x - (u_\infty/a_\infty)r$, where $a_\infty = (\gamma p_\infty/\rho_\infty)^{1/2}$ is the sound speed. For r not too far from the jet, the last term of Eq. (12) should be retained. Let us change the independent variables of Eqs. (11) and (12) to ξ and r. The equations become

$$u_\infty \frac{\partial v'_r}{\partial \xi} + \frac{1}{\rho_\infty}\frac{\partial p'}{\partial r} - \frac{u_\infty}{\rho_\infty a_\infty}\frac{\partial p'}{\partial \xi} = 0 \tag{13}$$

$$u_\infty \frac{\partial p'}{\partial \xi} + \gamma p_\infty\left(\frac{\partial v'_r}{\partial r} - \frac{u_\infty}{a_\infty}\frac{\partial v'_r}{\partial \xi} + \frac{v'_r}{r}\right) = 0 \tag{14}$$

Because u_∞ is small, the solution may be expanded as a series in u_∞, that is,

$$v'_r = v_0 + u_\infty v_1 + u_\infty^2 v_2 + \cdots$$

$$p' = p_0 + u_\infty p_1 + u_\infty^2 p_2 + \cdots \tag{15}$$

It is easy to find, by substituting Eq. (15) into Eqs. (13) and (14) and after some simple integrations, the following formulas for the first two terms of Eq. (15):

$$v_0 = \frac{\hat{v}_0(\xi)}{r}, \qquad v_1 = \frac{1}{a_\infty}\frac{\mathrm{d}\hat{v}_0}{\mathrm{d}\xi}$$

$$p_0 = 0, \qquad p_1 = -\rho_\infty \frac{\mathrm{d}\hat{v}_0}{\mathrm{d}\xi}(\ell n\, r) \tag{16}$$

where $\hat{v}_0(\xi)$ is an arbitrary function. By the differentiation of Eqs. (15) and (16) to eliminate $\hat{v}_0(\xi)$, it is straightforward to derive the boundary conditions

$$\frac{u_\infty}{a_\infty}\frac{\partial v'_r}{\partial x} + \frac{\partial v'_r}{\partial r} + \frac{v'_r}{r} = 0 \tag{17}$$

$$\frac{u_\infty}{a_\infty}\frac{\partial p'}{\partial x} + \frac{\partial p'}{\partial r} - \frac{p'}{r(\ell n\, r)} = 0 \tag{18}$$

In summary, the boundary conditions for all of the flow variables, to be imposed in the jet near field, are

$$u = u_\infty, \qquad \left(\frac{u_\infty}{a_\infty}\frac{\partial}{\partial x}+\frac{\partial}{\partial r}+\frac{1}{r}\right)\begin{bmatrix} v \\ w \end{bmatrix} = 0$$

$$\left(\frac{u_\infty}{a_\infty}\frac{\partial}{\partial x}+\frac{\partial}{\partial r}-\frac{1}{r(\ell n\, r)}\right)\begin{bmatrix} p - p_\infty \\ T - T_\infty \end{bmatrix} = 0, \qquad k = \varepsilon = 0 \tag{19}$$

III. Mean Flow Refraction Effects

To account for mean flow refraction effect on the radiated sound, Tam and Auriault[1] made use of the adjoint Green's function. The computation of the adjoint Green's function for axisymmetric jets was discussed in detail by Tam and Auriault.[18] Here the method is generalized for application to nonaxisymmetric jets.

Jets evolve slowly in the flow direction. A natural approximation is to regard the mean flow as locally parallel. Tam and Auriault[18] investigated the accuracy of the locally parallel flow approximation and concluded that the approximation would yield good results outside the cone of silence. Because fine-scale turbulence noise is dominant in the sideline and upstream directions that are not in the cone of silence, the locally parallel flow approximation will be used throughout this work.

A. Adjoint Green's Function as Solution of Scattering Problem

Let $\bar{u}(y, z)$, $\bar{\rho}(y, z)$, and $\bar{p}(y, z)$ be the mean flow velocity, density, and pressure distribution of a jet. Let us consider the time harmonic adjoint Green's function, denoted by a subscript a. The governing equations for the adjoint Green's function are (see Ref. 18)

$$-i\omega u_a - \bar{u}\frac{\partial u_a}{\partial x} - \gamma\bar{p}\frac{\partial p_a}{\partial x} = 0$$

$$-i\omega v_a - \bar{u}\frac{\partial v_a}{\partial x} + \frac{\partial \bar{u}}{\partial y}u_a - \gamma\bar{p}\frac{\partial p_a}{\partial y} = 0$$

$$-i\omega w_a - \bar{u}\frac{\partial w_a}{\partial x} + \frac{\partial \bar{u}}{\partial z}u_a - \gamma\bar{p}\frac{\partial p_a}{\partial z} = 0$$

$$-i\omega p_a - \bar{u}\frac{\partial p_a}{\partial x} - \frac{\partial}{\partial x}\left(\frac{u_a}{\bar{\rho}}\right) - \frac{\partial}{\partial y}\left(\frac{v_a}{\bar{\rho}}\right) - \frac{\partial}{\partial z}\left(\frac{w_a}{\bar{\rho}}\right) = \frac{1}{2\pi}\delta(\boldsymbol{x}-\boldsymbol{x}_0) \tag{20}$$

where $\boldsymbol{x}_0$ is the far-field observation point at which jet noise is to be measured.

Outside the jet, $\bar{u}$ is zero. It is straightforward to find from Eq. (20) that p_a satisfies the equation

$$\nabla^2 p_a + \left(\omega^2/a_\infty^2\right)p_a = \left(i\omega/2\pi a_\infty^2\right)\delta(\boldsymbol{x}-\boldsymbol{x}_0) \tag{21}$$

The solution of Eq. (21) is

$$p_a = \frac{-i\omega}{8\pi^2 a_\infty^2}\frac{\exp[i(\omega/a_\infty)|\boldsymbol{x}-\boldsymbol{x}_0|]}{|\boldsymbol{x}-\boldsymbol{x}_0|} \tag{22}$$

where $|\boldsymbol{x}-\boldsymbol{x}_0|$ is the distance between $\boldsymbol{x}$ and $\boldsymbol{x}_0$.

For convenience, let the spherical coordinates of $\boldsymbol{x}_0$ be (R, Θ, ϕ) (Fig. 1). The polar axis of the spherical coordinate system coincides with the x axis. Θ is the polar angle and ϕ is the azimuthal angle. Here our interest is confined to the far field, namely, $R \to \infty$. For large R, we have

$$|\boldsymbol{x}-\boldsymbol{x}_0| \simeq R - \boldsymbol{x}\cdot\boldsymbol{x}_0/R$$

$$= R - \cos\Theta x - \sin\Theta\cos\phi y - \sin\Theta\sin\phi z$$

By means of the preceding far-field approximation, it is easy to find, from Eq. (22) and the corresponding formulas for the velocity components, the solution for the adjoint Green's function, as $R \to \infty$, to be

$$\begin{bmatrix} u_a \\ v_a \\ w_a \\ p_a \end{bmatrix} = \frac{-i\omega}{8\pi^2 a_\infty^2 R}\begin{bmatrix} \rho_\infty a_\infty\cos\Theta \\ \rho_\infty a_\infty\sin\Theta\cos\phi \\ \rho_\infty a_\infty\sin\Theta\sin\phi \\ 1 \end{bmatrix} \times \exp[i(\omega/a_\infty)(R - \cos\Theta x - \sin\Theta\cos\phi y - \sin\Theta\sin\phi z)] \tag{23}$$

Now the adjoint Green's function of Eq. (20) may be found as a wave scattering problem by solving the homogeneous equation of Eq. (20) with Eq. (23) as the incident wave. This task is greatly simplified by noting that under the locally parallel flow approximation the coefficients of Eq. (20) are independent of x. Thus, the solution must have the same x dependence as the incident wave. That is,

$$u_a(x, y, z, \omega)\exp(-i\omega t) = \tilde{u}_a(y, z, t)\exp[-i(\omega/a_\infty)\cos\Theta x] \tag{24}$$

and similarly for the other variables.

When $\exp[-i(\omega/a_\infty)\cos\Theta x]$ is factored out and $-i\omega$ is replaced by $\partial/\partial t$ in Eq. (20) to make the equations time dependent, the adjoint Green's function problem becomes a two-dimensional sound scattering problem. The governing equations and the incident waves are as follows:

$$\frac{\partial \tilde{v}_a}{\partial t} + \frac{i\omega\bar{u}\cos\Theta}{a_\infty}\tilde{v}_a + \frac{\gamma\bar{p}\cos\Theta}{a_\infty - \bar{u}\cos\Theta}\frac{\partial \bar{u}}{\partial y}\tilde{p}_a - \gamma\bar{p}\frac{\partial \tilde{p}_a}{\partial y} = 0$$

$$\frac{\partial \tilde{w}_a}{\partial t} + \frac{i\omega\bar{u}\cos\Theta}{a_\infty}\tilde{w}_a + \frac{\gamma\bar{p}\cos\Theta}{a_\infty - \bar{u}\cos\Theta}\frac{\partial \bar{u}}{\partial z}\tilde{p}_a - \gamma\bar{p}\frac{\partial \tilde{p}_a}{\partial z} = 0$$

$$\frac{\partial \tilde{p}_a}{\partial t} + \frac{i\omega\bar{u}\cos\Theta}{a_\infty}\tilde{p}_a + \frac{i\omega}{a_\infty}\frac{\gamma\bar{p}\cos^2\Theta}{\bar{\rho}(a_\infty - \bar{u}\cos\Theta)}\tilde{p}_a - \frac{\partial}{\partial y}\left(\frac{\tilde{v}_a}{\bar{\rho}}\right) - \frac{\partial}{\partial z}\left(\frac{\tilde{w}_a}{\bar{\rho}}\right) = 0 \tag{25}$$

Outside the jet, the incident wave is

$$\begin{bmatrix} \tilde{v}_a \\ \tilde{w}_a \\ \tilde{p}_a \end{bmatrix} \to \frac{-i\omega}{8\pi^2 a_\infty^2 R}\begin{bmatrix} \rho_\infty a_\infty\sin\Theta\cos\phi \\ \rho_\infty a_\infty\sin\Theta\sin\phi \\ 1 \end{bmatrix} \times \exp[(i\omega/a_\infty)(R - \sin\Theta\cos\phi y - \sin\Theta\sin\phi z - a_\infty t)] \tag{26}$$

In deriving Eq. (25), the relationship

$$u_a = \frac{\gamma\bar{p}\cos\Theta}{a_\infty - \bar{u}\cos\Theta}p_a \tag{27}$$

which is the integral of the first equation of Eq. (20), has been used.

B. Numerical Solution

For a given mean flow $\bar{u}(y, z)$, $\bar{\rho}(y, z)$, and $\bar{p}(y, z)$, the sound scattering problem of Eqs. (25) and (26) may be solved computationally. For this purpose, Eq. (25) is discretized according to the seven-point stencil DRP scheme[8,19] in a rectangular computation domain as shown in Fig. 2. The outer boundary of the computation domain is taken to be where the mean flow $\bar{u}$ differs from u_∞ by 0.1% of u_j. This choice assures that a larger computation domain is used for x stations farther downstream from the nozzle exit. The mesh size is set by the smaller of the following two criteria. To ensure the DRP scheme has sufficient spatial resolution for the incident and

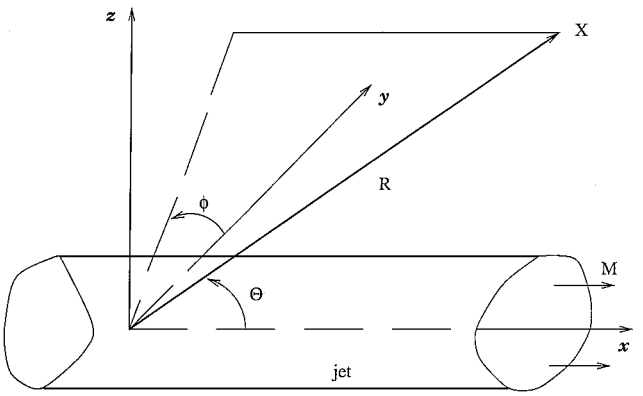

Fig. 1 Relationship between spherical coordinates (R, θ, ϕ) and the Cartesian coordinates.

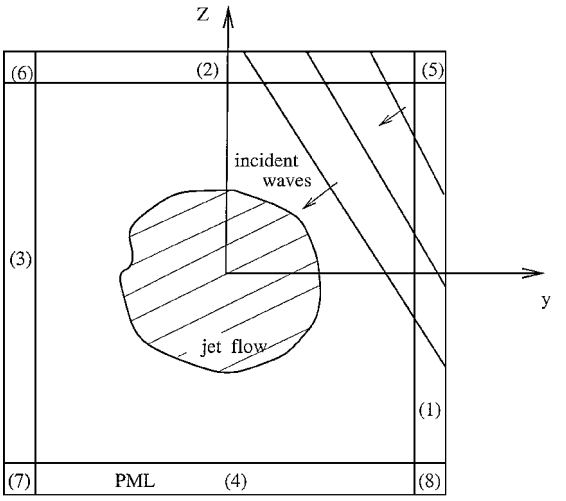

Fig. 2 Computational domain showing the jet flow, incident sound waves, and the PML.

the scattered acoustic waves, no less than seven mesh spacings per acoustic wavelength is used. That is, a finer mesh is automatically used for high-frequency waves. To make certain that the refraction of sound by the mixing layer of the jet is accurately computed, a minimum of eight mesh spacings is used per half-width of the layer. To eliminate spurious numerical waves that may inadvertently be generated at the boundaries of the computation domain, artificial selective damping terms[19,20] are added to the discretized equations. The artificial selective damping terms damp the short waves without affecting the physical (long) waves. The inverse mesh Reynolds number of the damping terms is given a value of 0.05. This value has been found to yield very satisfactory results.

As shown in Fig. 2, the computation domain is surrounded by a PML. The PML has a thickness of 15 mesh points. In this layer, the flow variables are split into two parts (the split variable method).[21] One part of the variables will be assigned the values of the incident wave given by Eq. (26). The other part is the scattered waves. The scattered waves are damped by the built-in damping of the PML.[22–24] The layer is called perfectly matched because, in principle, there is no reflected wave back into the computation domain. The construction of the PML is discussed in the Appendix.

For a given direction of radiation and frequency, the incident wave (26) is completely specified. To start the computation, initial conditions are required. In this work, the incident wave is used as the starting condition. The solution is marched in time until a time periodic state is attained. At this time, the maximum absolute value of $\tilde{p}_a$ over a cycle is measured at every point in the jet. This is the absolute value of the adjoint Green's function $|p_a|$ needed for noise computation.

IV. Comparisons with Experimental Measurements

Tam and Auriault[1] derived the following formula for the far-field noise spectrum, $S(R, \Theta, \phi, fD_j/u_j)$, in decibels per Strouhal number fD_j/u_j:

$$S\left(R, \Theta, \phi, \frac{fD_j}{u_j}\right) = 10\log\left[\frac{\tilde{S}(R, \Theta, \phi, f)}{p_{\text{ref}}^2 (D_j/u_j)}\right] \tag{28}$$

where

$$\tilde{S}(R, \Theta, \phi, f) = (4\pi)^2 \left(\frac{\pi}{\ell n\, 2}\right)^{\frac{3}{2}} \iiint_{\text{jet}} \frac{\hat{q}_s^2 \ell_s^3}{c^2 \tau_s} \times \left\{\frac{|p_a(\boldsymbol{x}_2, \boldsymbol{x}, \omega)|^2 \exp\left[-\omega^2 \ell_s^2 \big/ \bar{u}^2 (4\, \ell n\, 2)\right]}{1 + \omega^2 \tau_s^2 [1 - (\bar{u}/a_\infty)\cos\Theta]^2}\right\} d\boldsymbol{x}_2 \tag{29}$$

In Eqs. (28) and (29), $\boldsymbol{x}_2$ is the source point, $\boldsymbol{x}$ is the far-field measurement point with spherical coordinates (R, Θ, ϕ), $\omega = 2\pi f$ is the angular frequency, and p_{ref} is the reference pressure for the decibel scale. D_j and u_j are the fully expanded jet diameter and velocity. Here $\hat{q}_s$, ℓ_s, and τ_s are the intensity, spatial size, and decay time of the fine-scale turbulence. These quantities are related to k (the turbulence kinetic energy) and ε (the dissipation rate) of the k–ε turbulence model as follows:

$$\ell_s = c_\ell \ell = c_\ell \left(k^{\frac{3}{2}} \big/ \varepsilon\right), \qquad \tau_s = c_\tau \tau = c_\tau (k/\varepsilon) \tag{30}$$

$$\hat{q}_s^2 \big/ c^2 = A^2 q^2, \qquad q = \tfrac{2}{3}\bar{\rho} k \tag{31}$$

where $\bar{\rho}$ is the mean density of the jet flow at $\boldsymbol{x}_2$ and c_ℓ, c_τ, and A are the three empirical constants of the Tam and Auriault theory.[1] They are assigned the values of

$$c_\ell = 0.256, \qquad c_\tau = 0.233, \qquad A = 0.755 \tag{32}$$

In addition, $\bar{u}$ is the mean flow velocity at $\boldsymbol{x}_2$, a_∞ is the ambient sound speed, and $p_a(\boldsymbol{x}_2, \boldsymbol{x}, \omega)$ is the adjoint Green's function of the preceding section.

The first step in implementing formulas (28) and (29) is to compute the mean flow using Eq. (1), the parabolized RANS equations. To start the calculation at the nozzle exit, it is assumed that the mean flow is uniform, surrounded by a thin mixing layer with a Gaussian profile. The half-width of the mixing layer is taken to be 1.5–2.0% of the equivalent diameter D_{eq} of the nozzle. The equivalent diameter is the diameter of a circular nozzle with the same area. Experience indicates that a small variation of the initial half-width of the mixing layer has little effect on the radiated noise. It affects only slightly the high-frequency part of the spectrum.

It is well known that a nonaxisymmetric jet tends to become less asymmetric in the downstream direction. This is confirmed in the present numerical results. Figure 3 shows the computed contours of the axial velocity component of a Mach 2 jet at a temperature ratio 1.8 (reservoir to ambient temperature) from a rectangular nozzle of aspect ratio 7.6. The first quadrant is for the flow at $x = 1D_{\text{eq}}$ downstream. The second, third, and fourth quadrants are for the mean flow at $5D_{\text{eq}}$, $10D_{\text{eq}}$, and $15D_{\text{eq}}$ downstream. The contours clearly show the tendency to become more and more circular. Figure 4 shows a similar plot for a cold subsonic jet at Mach 0.8 from an aspect ratio 8 rectangular nozzle. Again the velocity contours tend to evolve into a circular shape. A comparison between Figs. 3 and 4 confirms the expectation that a subsonic rectangular jet would transition into a circular jet faster than a supersonic jet. This is not surprising because the axial scale for a jet is the core length. The potential core of a

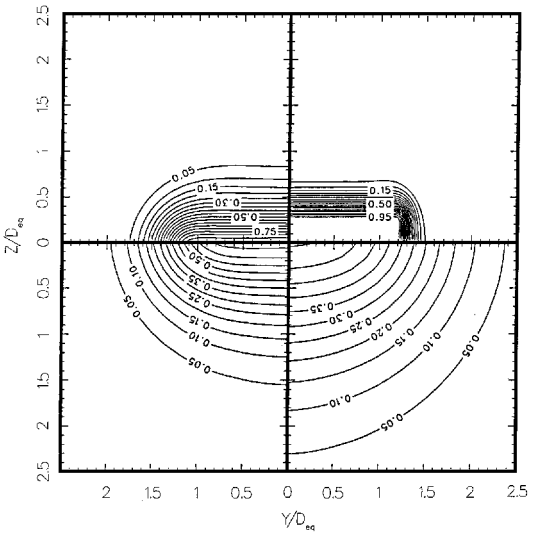

Fig. 3 Contours of the axial velocity component of a Mach 2 jet at temperature ratio 1.8 from a rectangular nozzle of aspect ratio 7.6; first, second, third, and fourth quadrant are for cross sections at X/D_{eq} = 1, 5, 10, and 15.

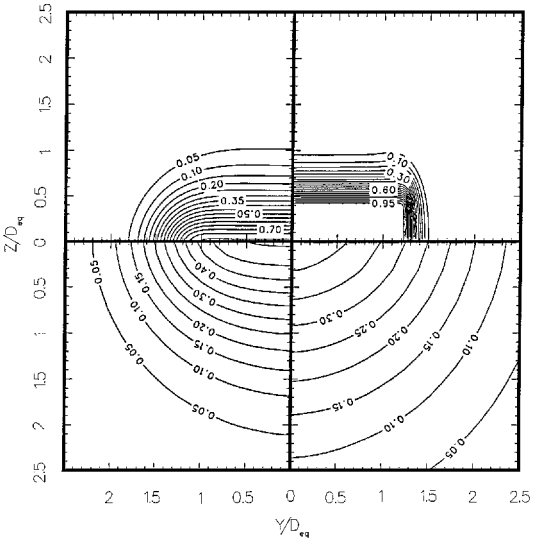

Fig. 4 Contours of the axial velocity component of a Mach 0.82 cold jet from a rectangular nozzle of aspect ratio 8; first, second, third, and fourth quadrant are for cross sections at X/D_{eq} = 1, 5, 10, and 15.

supersonic jet is much longer than that of a subsonic jet in terms of equivalent nozzle diameter.

Only a limited number of sets of nonaxisymmetric jet noise data are available for comparison with predictions. Here two sets of supersonic Mach number data, one from an elliptic jet of aspect ratio 3 and the other from a rectangular jet of aspect ratio 7.6, measured by Seiner et al.[2] at the Jet Noise Laboratory of the NASA Langley Research Center will be used. The design Mach number of the nozzles of these jets is 2.0. The data are of high quality, comparable to the axisymetric jet noise data used for comparison in Refs. 1 and 3. Tam and Zaman[25] measured subsonic jet noise spectra from an elliptic nozzle of aspect ratio 3 and rectangular nozzles of aspect ratios 3 and 8 along the major and minor axis directions. Because of the facility used is only semi-anechoic, the quality of the data is not as good but still acceptable. The preceding references are the experimental data available to us for comparisons with theoretical predictions.

Figures 5a–5c show comparisons between calculated and measured noise spectra for the aspect ratio 3, Mach 2, elliptic jet at a temperature ratio 1.0. The polar angle Θ (exhaust angle) of the measurement microphone is at 90 deg. Figure 5a is the spectrum measured in the major axis plane ($\phi = 90$ deg). Figure 5b is the noise spectrum radiated in the direction of the minor axis plane ($\phi = 0$ deg). Figure 5c is the noise spectrum at $\phi = 58$ deg.

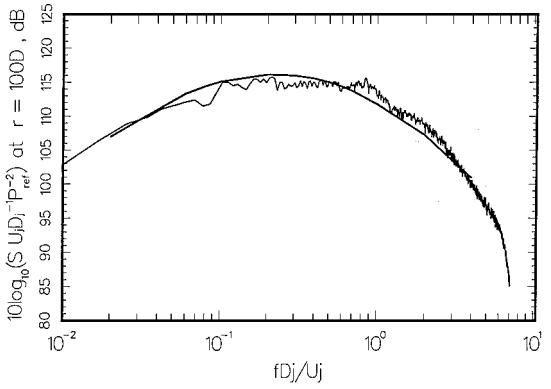

a) Major axis plane (ϕ = 90 deg)

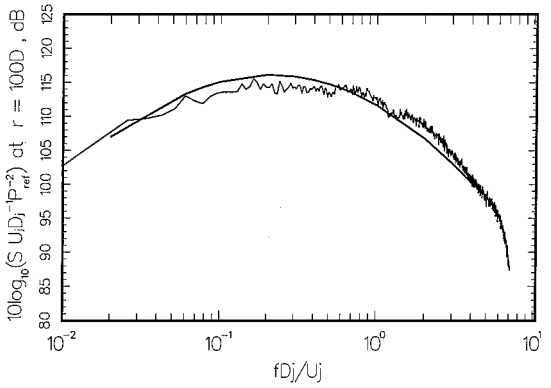

b) Minor axis plane (ϕ = 0 deg)

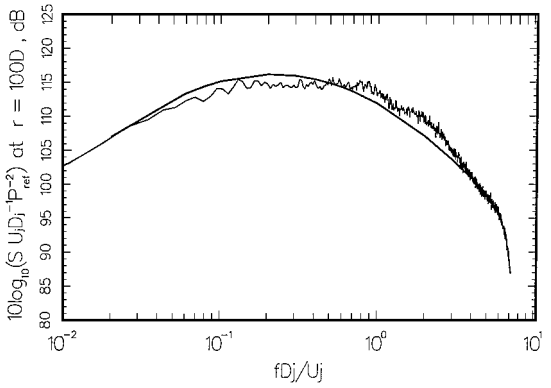

c) ϕ = 58 deg plane

Fig. 5 Noise spectra of an aspect ratio 3 elliptic jet at Mach 2.0, T_r/T_∞ = 1.0; data from Seiner et al.,[2] ——, computed spectra, Θ = 90 deg.

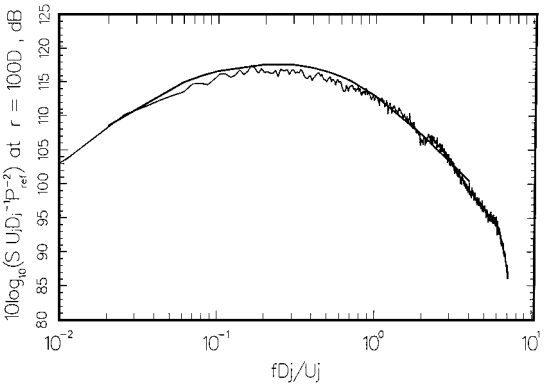

a) Major axis plane (ϕ = 90 deg)

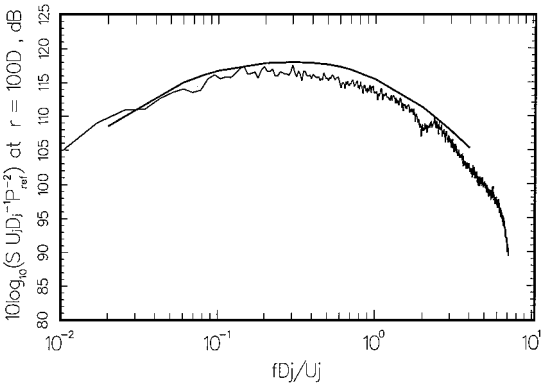

b) Minor axis plane (ϕ = 0 deg)

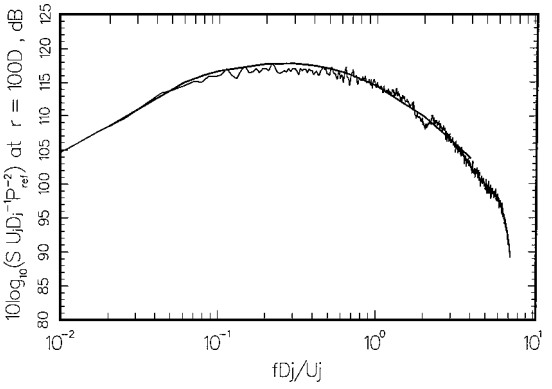

c) ϕ = 58 deg plane

Fig. 6 Noise spectra of an aspect ratio 3 elliptic jet at Mach 2.0, T_r/T_∞ = 1.0; data from Seiner et al.,[2] ——, computed spectra, Θ = 72 deg.

Figures 6a–6c are for the same jet as Fig. 5. Here Θ is 72 deg. Figure 6a is for radiation in the major axis plane ($\phi =$ 90 deg). Figure 6b is for radiation in the minor axis plane ($\phi =$ 0 deg). Figure 6c is the noise spectrum radiated in the $\phi = 58$ deg direction.

Figure 7 gives the comparisons between the calculated noise spectra and experimental measurements of a Mach 2, aspect ratio 7.6, rectangular jet at temperature ratio 1.8. The data are for the $\Theta = 90$ deg plane. In Fig. 7, curve a is the spectrum of the noise radiated in the major axis plane direction. In Fig. 7, curve b is the spectrum in the minor axis plane direction.

Figure 8 is for the same jet as Fig. 7. In this case the polar angle is $\Theta = 72$ deg. The full curve is the calculated noise spectrum in the major axis direction, $\phi = 90$ deg. The dotted curve is the predicted spectrum in the minor axis direction ($\phi = 0$ deg). It is quite clear that, at this polar angle, the directivity is asymmetric with more noise radiated in the minor axis plane. The main reason for the

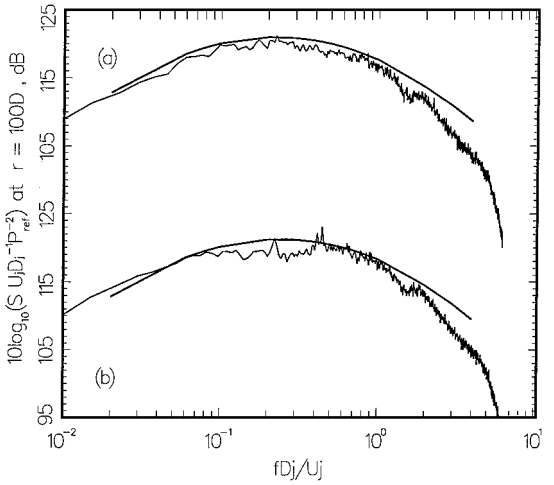

Fig. 7 Noise spectra of an aspect ratio 7.6 rectangular jet at Mach 2.0, T_r/T_∞ = 1.8; data from Seiner et al.,[2] ——, computed spectra; Θ = 90 deg: major axis plane (a) and minor axis plane (b).

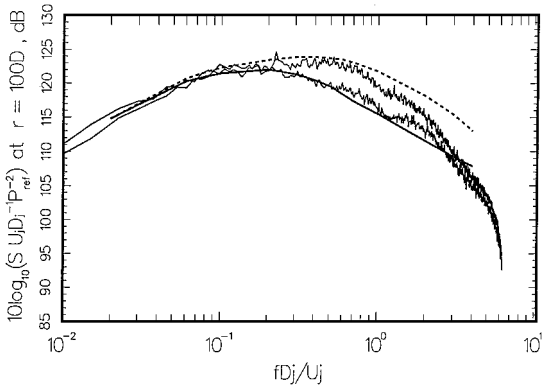

Fig. 8 Noise spectra of an aspect ratio 7.6 rectangular jet at Mach 2.0, T_r/T_∞ = 1.8; data from Seiner et al.,[2] Θ = 72 deg: computed spectra ——, major axis plane and - - - -, minor axis plane.

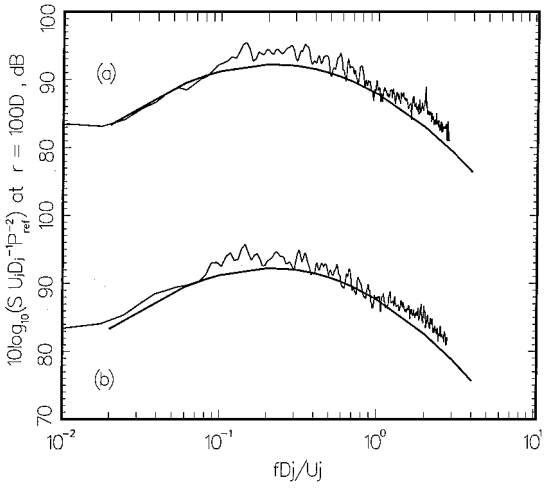

Fig. 9 Noise spectra of an aspect ratio 3 elliptic jet at Mach 0.82, T_r/T_∞ = 1.0; data from Tam and Zaman,[25] ——, computed spectra, Θ = 90 deg: major axis plane (a) and minor axis plane (b).

asymmetry is the mean flow refraction effect. Surrounding the two ends of the major axis of a large aspect ratio rectangular jet are thick mixing layers. They cause strong refraction to sound radiation. This contributes to a reduction of noise radiation in these directions. As can be seen, the calculated results seem to follow the measured data except at very high frequencies.

Figure 9 shows the noise spectra for the aspect ratio 3 elliptic jet at temperature ratio 1.0 and Mach number 0.82 measured by Tam and

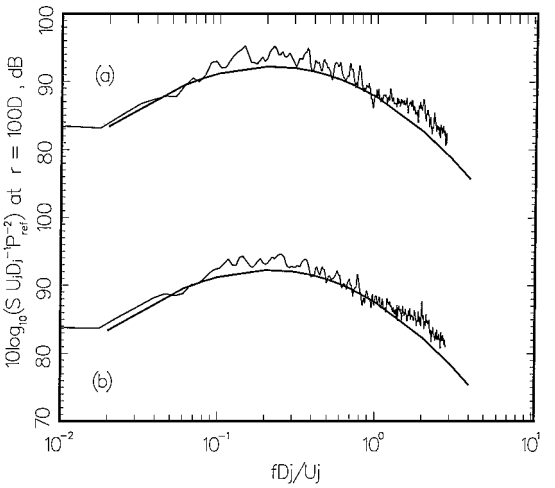

Fig. 10 Noise spectra of an aspect ratio 3 rectangular jet at Mach 0.82, T_r/T_∞ = 1.0; data from Tam and Zaman,[25] ——, computed spectra, Θ = 90 deg: major axis plane (a) and minor axis plane (b).

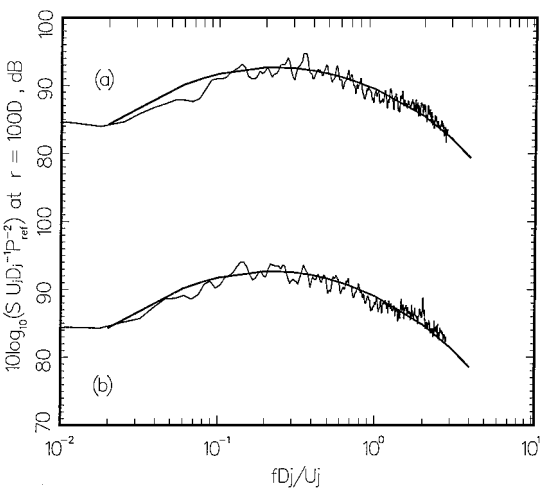

Fig. 11 Noise spectra of an aspect ratio 8.0 rectangular jet at Mach 0.82, T_r/T_∞ = 1.0; data from Tam and Zaman,[25] ——, computed spectra, Θ = 90 deg: major axis plane (a) and minor axis plane (b).

Zaman.[25] Shown in Fig. 9 also are the calculated noise spectra. Curve a is the noise spectrum at $\Theta = 90$ deg and $\phi = 90$ deg (the major axis plane). Curve b is the noise spectrum at $\Theta = 90$ deg and $\phi = 0$ deg (the minor axis plane). Figure 10 shows the measured spectra for a similar rectangular jet (same aspect ratio, temperature ratio, and Mach number). The calculated noise spectra are also provided.

Finally, Fig. 11 shows the noise spectra of a large aspect ratio rectangular jet (aspect ratio 8) at Mach 0.82 and temperature ratio 1.0. The smooth curves in Fig. 11 are the calculated noise spectra. Both the calculated and measured spectra are for noise radiation in the $\Theta = 90$ deg plane. Curve a is for radiation in the major axis plane ($\phi = 90$ deg) whereas curve b is for radiation in the minor axis plane ($\phi = 0$ deg). Overall, there is good agreement between the spectrum calculated by Eqs. (28) and (29) of the Tam and Auriault theory[1] and the measured spectrum in each of the described cases.

It is known that at high frequencies, for example, above 20–30 kHz, atmospheric correction becomes important and must be taken into account. For a Mach 2.0 jet from a 2-in. (5.08-cm) equivalent diameter nozzle, this corresponds to a Strouhal number 2.0–3.0. This should be considered the upper limit in the present comparisons with experiments.

V. Conclusions

In this work, the semi-empirical jet noise theory of Tam and Auriault[1] is extended to nonaxisymmetric jets. A set of improved numerical boundary conditions for the parabolized RANS equations

is developed. This new set of boundary conditions makes it possible to compute the jet mean flow and the physical variables of the k–ε turbulence model using a smaller computation domain. The adjoint Green's function needed to account for mean flow refraction effect is reformulated into the solution of a two-dimensional acoustic scattering problem. It is demonstrated that the solution can be found accurately and efficiently by time marching the solution to a periodic state by the DRP scheme. Good agreements are found between computed noise spectra and experimental measurements. It is believed that this is the first time noise spectra of nonaxisymmetric jets are calculated with good accuracy.

As a part of the present investigation, a large number of nonaxisymmetric jet noise spectra in the $\Theta = 90$ deg plane have been examined. It appears that the spectra are nearly independent of the azimuthal angle. In the 90-deg plane, there is no noise source convection effect nor mean flow refraction effect. Thus, it appears that fine-scale turbulence noise, by itself, is quite isotropic. In other words, the noise sources behave like monopoles.

For noise radiated in the downstream direction, the nonaxisymmetric mean flow exerts a strong influence on the noise spectrum. For instance, in the case of a rectangular or elliptic jet with large aspect ratio, there is a much thicker shear layer on the smaller dimension sides of the jet. Refraction by the shear layer reduces the radiation of high-frequency sound. This immediately leads to a nonaxisymmetric sound field (at a fixed polar angle) with more noise radiated in the minor axis plane. This is borne out in both the numerical results and experimental measurements.

Appendix: Perfectly Matched Layer Absorbing Boundary Condition

Berenger[22] invented the PML as absorbing boundary condition for computational electromagnetics. Hu[23] applied the idea to acoustic problems. Tam et al.[24] showed that, in the case of Euler equations with flow normal to the perfectly matched layer, the PML equations have unstable solutions that can, however, be stabilized by the addition of appropriate artificial selective damping. In all of the works mentioned, the waves are nondispersive. Equation (25) of the adjoint Green's function, however, supports dispersive waves. The purpose of this Appendix is to show how a PML absorbing boundary condition can be formulated that will absorb all outgoing dispersive waves of Eq. (25). Furthermore, it will be shown that the PML equations are stable.

Outside the jet, $\bar{u} = 0$, $\bar{\rho} = \rho_\infty$, Eq. (25) reduces to

$$\frac{\partial \tilde{v}_a}{\partial t} - \gamma p_\infty \frac{\partial \tilde{p}_a}{\partial y} = 0 \tag{A1}$$

$$\frac{\partial \tilde{w}_a}{\partial t} - \gamma p_\infty \frac{\partial \tilde{p}_a}{\partial z} = 0 \tag{A2}$$

$$\frac{\partial \tilde{p}_a}{\partial t} + i\omega \cos^2\Theta \tilde{p}_a - \frac{1}{\rho_\infty}\left(\frac{\partial \tilde{v}_a}{\partial y} + \frac{\partial \tilde{w}_a}{\partial z}\right) = 0 \tag{A3}$$

Let us look for plane wave solutions of Eqs. (A1–A3) in the form

$$\begin{bmatrix} \tilde{v}_a \\ \tilde{w}_a \\ \tilde{p}_a \end{bmatrix} = \begin{bmatrix} \hat{v} \\ \hat{w} \\ \hat{p} \end{bmatrix} \exp[i(\alpha y + \beta z - \Omega t)] \tag{A4}$$

By substitution of Eq. (A4) into Eqs. (A1–A3), it is easy to find

$$\hat{v} = -\left(\frac{\alpha}{\Omega}\right)\gamma p_\infty \hat{p} \tag{A5}$$

$$\hat{w} = -\left(\frac{\beta}{\Omega}\right)\gamma p_\infty \hat{p} \tag{A6}$$

$$\left(1 - \frac{\omega \cos^2\Theta}{\Omega}\right)\hat{p} + \frac{1}{\rho_\infty}\left(\frac{\alpha}{\Omega}\right)\hat{v} + \frac{1}{\rho_\infty}\left(\frac{\beta}{\Omega}\right)\hat{w} = 0 \tag{A7}$$

Equations (A5–A7) are homogeneous equations. For nontrivial solution, the determinant of the coefficient matrix of these equations, when written in a matrix form, must be equal to zero. This gives the dispersion relation that may be simplified to

$$\Omega^2 - \omega\Omega \cos^2\Theta - a_\infty^2(\alpha^2 + \beta^2) = 0 \tag{A8}$$

For a wave of a given frequency Ω, its wave numbers, which are often referred to as the eigenvalues of the homogeneous system, are given by the roots of Eq. (A8). On solving Eq. (A8) for α, one finds

$$\alpha_\pm = \pm\left(\Omega^2 - \omega\Omega\cos^2\Theta - a_\infty^2\beta^2\right)^{\frac{1}{2}} \Big/ a_\infty \tag{A9}$$

When Eq. (A8) is differentiated and Eq. (A9) is used, the group velocity of the acoustic wave in the x direction is found:

$$\frac{\partial \Omega}{\partial \alpha} = \pm \frac{2a_\infty\left(\Omega^2 - \omega\Omega\cos^2\Theta - a_\infty^2\beta^2\right)^{\frac{1}{2}}}{2\Omega - \omega\cos^2\Theta} \tag{A10}$$

The $\pm$ sign in Eq. (A10) corresponds to $\alpha_\pm$. Now the group velocity is a function of frequency or wave number. Hence, the waves are dispersive.

For $\Omega > 0$, so that $\alpha_\pm$ are real (propagating waves), Ω must be larger than $\omega\cos^2\Theta$. That is, the denominator of Eq. (A10) is positive. Thus, α_+ is the right-propagating wave (positive group velocity), and α_- is the left-propagating wave (negative group velocity). For $\Omega < 0$, it is the other way around. In other words, for the right-propagating wave, we have $\alpha/\Omega > 0$ and $\alpha/\Omega < 0$ for the left-propagating wave.

Now let us consider PML 1 of Fig. 2. When standard PML formulation is followed, the governing equations and variables in layer 1 are

$$\tilde{v}_a = v_1, \qquad \tilde{w}_a = w_2, \qquad \tilde{p}_a = p_1 + p_2 \tag{A11}$$

$$\frac{\partial v_1}{\partial t} + \sigma v_1 - \gamma p_\infty \frac{\partial (p_1 + p_2)}{\partial y} = 0 \tag{A12}$$

$$\frac{\partial w_2}{\partial t} - \gamma p_\infty \frac{\partial (p_1 + p_2)}{\partial z} = 0 \tag{A13}$$

$$\frac{\partial p_1}{\partial t} + \sigma p_1 - \frac{1}{\rho_\infty}\frac{\partial v_1}{\partial y} = 0 \tag{A14}$$

$$\frac{\partial p_2}{\partial t} + i\omega\cos^2\Theta(p_1 + p_2) - \frac{1}{\rho_\infty}\frac{\partial w_2}{\partial z} = 0 \tag{A15}$$

Plane wave solutions of Eqs. (A12–A15) that match the frequency and traverse wave numbers of wave solution (A4) of the adjoint equations at the PML interface have the form

$$\begin{bmatrix} v_1 \\ w_2 \\ p_1 \\ p_2 \end{bmatrix} = \begin{bmatrix} \hat{v}_1 \\ \hat{w}_2 \\ \hat{p}_1 \\ \hat{p}_2 \end{bmatrix} \exp[i(\kappa y + \beta z - \Omega t)] \tag{A16}$$

By substitution of Eq. (A16) into Eqs. (A12–A15), it is straightforward to derive

$$\hat{v}_1 = -\frac{\kappa}{(\Omega + i\sigma)}\gamma p_\infty(\hat{p}_1 + \hat{p}_2) \tag{A17}$$

$$\hat{w}_2 = -\frac{\beta}{\Omega}\gamma p_\infty(\hat{p}_1 + \hat{p}_2) \tag{A18}$$

$$\hat{p}_1 = -\frac{\kappa}{\rho_\infty(\Omega + i\sigma)}\hat{v}_1 \tag{A19}$$

$$\left(1 - \frac{\omega}{\Omega}\cos^2\Theta\right)(\hat{p}_1 + \hat{p}_2) + \frac{1}{\rho_\infty}\frac{\kappa}{\Omega + i\sigma}\hat{v}_1 + \frac{1}{\rho_\infty}\frac{\beta}{\Omega}\hat{w}_2 = 0 \tag{A20}$$

Just as in the case of algebraic system (A5–A7), Eqs. (A17–A20) form an eigenvalue problem with κ as the eigenvalue. On comparing the two eigenvalue systems, it is clear that they are identical: same eigenvalue and eigenfunction. The wave numbers of the two problems are related by

$$\alpha/\Omega = \kappa/(\Omega + i\sigma)$$

or

$$\kappa = \alpha + i\sigma(\alpha/\Omega) \tag{A21}$$

That the eigenfunctions of the two systems are the same allows the incident wave to be completely transmitted without reflection at the PML interface. The transmitted wave has the y dependence of the form

$$\exp(i\kappa y) = \exp[i\alpha y - \sigma(\alpha/\Omega)y] \tag{A22}$$

Because $(\alpha/\Omega) > 0$ for the right-propagating wave, the transmitted wave is damped as it propagates through the PML.

Finally, to show that the PML equations are stable, it is easy to find that the dispersion relation of Eqs. (A11–A15) is

$$F \equiv \left(\Omega^2 - \omega\Omega\cos^2\Theta - \frac{a_\infty^2\kappa^2\Omega^2}{(\Omega + i\sigma)^2}\right) = a_\infty^2\beta^2 \tag{A23}$$

It can be shown, following Ref. 24 and using the definition of F defined by Eq. (A23), that the upper-half Ω plane is mapped into the entire complex F plane except for the positive real axis. Because $a_\infty^2\beta^2 > 0$, the right-hand side of Eq. (A23), is real and positive, it follows that there is no solution of Eq. (A23) with Ω in the upper-half Ω plane. This ensures that the system of PML equations has no unstable solution.

Acknowledgments

This work was supported by NASA Langley Research Center Grant NAG 1-2145, and computer time on a SGI Origin 2200 computer was provided by the Department of Mathematics, Florida State University.

References

[1]Tam, C. K. W., and Auriault, L., "Jet Mixing Noise from Fine Scale Turbulence," *AIAA Journal*, Vol. 37, No. 2, 1999, pp. 145–153.

[2]Seiner, J. M., Ponton, M. K., Jansen, B. J., and Lagen, N. T., "The Effects of Temperature on Supersonic Jet Noise Emission," AIAA Paper 92-2046, May 1992.

[3]Tam, C. K. W., Golebiowski, M., and Seiner, J. M., "On the Two Components of Turbulent Mixing Noise from Supersonic Jets," AIAA Paper 96-1716, May 1996.

[4]Tam, C. K. W., Pastouchenko, N., and Auriault, L., "Effects of Forward Flight on Jet Mixing Noise from Fine Scale Turbulence," *AIAA Journal*, Vol. 39, No. 7, 2001, pp. 1261–1269.

[5]Norum, T. D., and Brown, M. C., "Simulated High Speed Flight Effects on Supersonic Jet Noise," AIAA Paper 93-4388, Oct. 1993.

[6]Plumblee, H. E., "Effects of Forward Velocity on Turbulent Jet Mixing Noise," NASA CR-2702, 1976.

[7]Thies, A. T., and Tam, C. K. W., "Computation of Turbulent Axisymmetric and Nonaxisymmetric Jet Flows Using the k–ε Model," *AIAA Journal*, Vol. 34, No. 2, 1996, pp. 309–316.

[8]Tam, C. K. W., and Webb, J. C., "Dispersion-Relation-Preserving Finite Difference Schemes for Computational Acoustics," *Journal of Computational Physics*, Vol. 107, Aug. 1993, pp. 262–281.

[9]Goldstein, M. E., "The Low Frequency Sound from Multipole Sources in Axisymmetric Shear Flows," *Journal of Fluid Mechanics*, Vol. 70, 1975, pp. 595–604.

[10]Goldstein, M. E., "The Low Frequency Sound from Multipole Sources in Axisymmetric Shear Flows, Part 2," *Journal of Fluid Mechanics*, Vol. 75, 1976, pp. 17–28.

[11]Balsa, T. F., "The Far Field of High Frequency Convected Singularities in Sheared Flows with an Application to Jet Noise Prediction," *Journal of Fluid Mechanics*, Vol. 74, 1976, pp. 193–208.

[12]Goldstein, M. E., "High Frequency Sound Emission from Moving Point Multipole Sources Embedded in Arbitrary Transversely Sheared Mean Flows," *Journal of Sound and Vibration*, Vol. 80, 1982, pp. 499–522.

[13]Durbin, P. A., "High Frequency Green's Function for Aerodynamic Noise in Moving Media, Part I: General Theory," *Journal of Sound and Vibration*, Vol. 91, 1983, pp. 519–525.

[14]Durbin, P. A., "High Frequency Green's Function for Aerodynamic Noise in Moving Media, Part II: Noise from a Spread Jet," *Journal of Sound and Vibration*, Vol. 91, 1983, pp. 527–538.

[15]Khavaran, A., and Krejsa, E. A., "Propagating of High-Frequency Jet Noise Using Geometric Acoustics," AIAA Paper 93-0147, 1993.

[16]Khavaran, A., and Krejsa, E. A., "Refraction of High-Frequency Jet Noise in an Arbitrary Jet Flow," AIAA Paper 94-0139, 1994.

[17]Khavaran, A., "Role of Anisotrophy in Turbulent Mixing Noise," *AIAA Journal*, Vol. 37, No. 7, 1999, pp. 832–841.

[18]Tam, C. K. W., and Auriault, L., "Mean Flow Refraction Effects on Sound Radiated from Localized Sources in a Jet," *Journal of Fluid Mechanics*, Vol. 370, 1998, pp. 149–174.

[19]Tam, C. K. W., "Computational Aeroacoustics: Issues and Methods," *AIAA Journal*, Vol. 33, No. 10, 1995, pp. 1788–1796.

[20]Tam, C. K. W., Webb, J. C., and Dong, Z., "A Study of the Short Wave Components in Computation Acoustics," *Journal of Computational Acoustics*, Vol. 1, March 1993, pp. 1–30.

[21]Tam, C. K. W., "Advances in Numerical Boundary Conditions for Computational Aeroacoustics," *Journal of Computational Acoustics*, Vol. 6, Dec. 1998, pp. 377–402.

[22]Berenger, J. P., "A Perfectly Matched Layer for the Absorption of Electromagnetic Waves," *Journal of Computational Physics*, Vol. 114, 1994, pp. 185–200.

[23]Hu, F. Q., "On Absorbing Boundary Conditions for Linearized Euler Equations by a Perfectly Matched Layer," *Journal of Computational Physics*, Vol. 129, 1996, pp. 201–219.

[24]Tam, C. K. W., Auriault, L., and Cambuli, F., "Perfectly Matched Layer as an Absorbing Boundary Condition for the Linearized Euler Equations in Open and Ducted Domains," *Journal of Computational Physics*, Vol. 144, July 1998, pp. 213–234.

[25]Tam, C. K. W., and Zaman, K. B. M. Q., "Subsonic Jet Noise from Nonaxisymmetric and Tabbed Nozzles," *AIAA Journal*, Vol. 38, No. 4, 2000, pp. 592–599.

W. J. Devenport
Associate Editor